Journal of Quantitative Spectroscopy & Radiative Transfer 353 (2026) 109857

Contents lists available at ScienceDirect

Journal of Quantitative Spectroscopy and Radiative Transfer

journal homepage: www.elsevier.com/locate/jqsrt

Rotational investigation of Biarylic Thienyl Pyridines and their Monohydrates: The role of the S···N intramolecular interaction

Domingo Heras [a], Wenqin Li [a,b], Ibon Alkorta [c], Ruth Pinacho [d], Lourdes Enríquez [d], J. Emiliano Rubio [d], Cristóbal Pérez [a], Alberto Lesarri [a,*]

[a] Departamento de Química Física y Química Inorgánica, Facultad de Ciencias – I.U. CINQUIMA, Universidad de Valladolid, Paseo de Belén 7, 47011 Valladolid, Spain
[b] Astrophysik/I. Physikalisches Institut, Universität zu Köln, Zülpicher Str. 77, 50937 Köln, Germany
[c] Instituto de Química Médica, CSIC, Juan de la Cierva 3, 28006 Madrid, Spain
[d] Departamento de Electrónica, Escuela Técnica Superior de Ingenieros de Telecomunicación, Universidad de Valladolid, Paseo de Belén 11, 47011 Valladolid, Spain

ARTICLE INFO

Keywords:
Thienyl pyridines
Intermolecular aggregates
Microsolvation
Rotational spectroscopy
Non-covalent interactions
Electronic density shift

ABSTRACT

We used jet-cooled broadband rotational spectroscopy and quantum mechanical calculations to study the potential energy surface, molecular structure and intra- and intermolecular interactions of the biarylic thienyl pyridines of 2-(2-thienyl)pyridine and 2-(2-pyridyl)benzothiophene and their monohydrates. Two isomers of the bare molecules were identified in the gas phase, characterized by planar structures and *zusammen* (*Z*) or *entgegen* (*E*) orientations around the ring junction. A single *Z*-isomer was observed for both monohydrates, primary stabilized by a hydroxyl-to-nitrogen (O-H···N) hydrogen bond and secondary C-H···O interactions. The computational study included D3 dispersion-corrected hybrid (B3LYP) and double hybrid (B2PLYP) density functional methods, with additional calculations at the RI-MP2 and DLPNO-CCSD(T) levels. NBO calculations examined the donor-acceptor hyperconjugative effects involving the nitrogen and sulfur atoms, suggesting that their participation in the larger stability of the *Z* form is not decisive and may involve other intramolecular interactions. In particular, examination of the electronic density shifts (EDS) further suggests that non-covalent N···S chalcogen interactions partially contribute to the preference for the *Z* conformation.

1. Introduction

Recent advances in chirped-pulsed microwave excitation [1,2] have expanded the applicability of rotational spectroscopy, including challenging areas such as chiral recognition [3–5] and isotopic-resolved analysis [6–8]. In addition, rotational investigations on larger weakly-bound complexes [9–11] now offer detailed insight into multiple intermolecular interactions which may help modelling the ligand-host binding properties operating in biomedicine and biotechnology.

In this article we study two asymmetric biarylic thienyl pyridines, specifically 2-(2-thienyl)pyridine (TP) and 2-(2-pyridyl)benzothiophene (PBT, see Fig. 1) and their monohydrates, yielding a comprehensive description of the potential energy surface (PES), spectroscopic properties and intra- and intermolecular interactions. TP and PBT are ring assemblies connected by a single bond, permitting different orientations between the two connected rings. Both molecules are structurally relevant because of their potential applications in materials science and pharmaceuticals. Thiophene-containing compounds are central to the biological activity of many medicinal agents [12–16]. These molecules also act as ligands for diverse metal centres [17,18], with several derivatives active in photoinduced processes [19,20], bioimaging [21] and in catalysing organic transformations [22].

The stereochemistry of biaryl compounds [23] has been studied in the context of atropisomerism [24] and formation of molecular rotors [25], and depends on the type and position of molecular substituents around the ring junction. In TP and PBT the orientation of the fused aromatic rings will affect the separation and the plausible interaction between the nitrogen and sulfur atoms, which in turn influences the electron density distribution, polarizability, and overall dipole moment —key factors that affect the potential energy surface and chemical behaviour.

A few ring assemblies and biaryl compounds have been previously

This article is dedicated to the memory of Prof. Dr. Mikhail Yu. Tretyakov (Institute of Applied Physics, Russian Academy of Sciences), for his contributions to science.

* Corresponding author.
E-mail address: alberto.lesarri@uva.es (A. Lesarri).

https://doi.org/10.1016/j.jqsrt.2026.109857
Received 23 December 2025; Received in revised form 1 February 2026; Accepted 2 February 2026
Available online 3 February 2026

studied with rotational resolution, including biphenols [26], nicotine alkaloids [27,28] and antipyretics [29]. These studies show delicate intramolecular equilibria controlled by electronic or steric interactions. In this work we will examine if the presence of the nitrogen and sulfur heteroatoms may condition the molecular structure of the assembly and whether the insertion of a water molecule might distort the intramolecular interactions and structure of the monomers. We are unaware of previous spectroscopic investigations of the title compounds in the gas phase.

2. Experimental and computational methods

The samples of TP (m.p. 61-63°C) and PBT (m.p. 123-127°C) were purchased commercially and required no further purification. The samples were vaporized inside a pulsed injection valve (TP: 80°C, PBT: 175°C), pressurized (0.2 MPa) and later expanded near-adiabatically into an evacuated (0.1 mPa) vacuum chamber, creating a pulsed supersonic jet. A He-Ar mixture with a 1:1 composition was used as carrier gas. The advantages of such a mixture are discussed elsewhere [30]. For observation of the monohydrates a water receptacle was inserted into the gas line.

The rotational spectra were recorded with a chirped-pulse Fourier transform microwave spectrometer operating in the 2-8 GHz frequency range [31,32]. The radiation source is an arbitrary waveform generator (25 GS/s), emitting a short (4 μs) chirp pulse covering the full frequency range. In this experiment eight chirped pulses were used for each gas pulse. The excitation chirped pulses are amplified with a travelling-wave tube (300 W) and broadcasted perpendicularly into the jet. The resulting transient emission contains contributions from the rotational transitions of all polar species in the gas phase and is recorded with a digital oscilloscope (25 GS/s). The time domain is finally transformed into the frequency domain spectrum with a Fourier transformation. The total experiment included 1 M cycles of operation. The uncertainty of the frequency measurements is below 10 kHz. Typical linewidths (full width at half maximum) are ca. 100 kHz.

Several computational methods were used in this work. The potential energy surface of the monomers is monodimensional and could be explored systematically using density functional theory (DFT). For the monohydrates, the initial conformational search used a semiempirical method (GFN2-xTB [33]) implemented in CREST [34]. Geometry optimizations were first carried out with the hybrid B3LYP-D3(BJ) method [35,36], including Grimme's D3 dispersion [37] and Becke–Johnson damping [38] (ultrafine integration grid and tight self-consistent field convergence criteria). To refine energetic and structural parameters, the most stable conformers were further reoptimized using the double-hybrid B2PLYP-D3(BJ) method [39], which includes perturbative second-order correlation contributions. These calculations used the def2-TZVP basis set and run in Gaussian16 [40].

For better benchmarking of the interaction energies, RI-SCS-MP2/cc-pVTZ calculations [41] were carried out employing the resolution-of-the-identity approximation. Finally, DLPNO-CCSD(T) calculations [42,43] were performed using the aug-cc-pVTZ basis set, implemented in ORCA [44] (TightPNO settings and default auxiliary basis sets for RI approximations).

A Natural Bond Orbital (NBO) analysis was performed to gain insight into donor–acceptor interactions and electronic delocalization, using the NBO program [45]. The non-covalent interactions were initially analyzed using the Non-Covalent Interaction (NCI) index, calculated from the reduced density gradient using the NCIPlot program [46]. Additionally, the Electron Density Shift (EDS) arising from the interaction between the substituent groups on the two aromatic rings was computed following the methodology described in Ref. [47]. The systems were partitioned along the C–C bond connecting the two rings, and methyl groups with hydrogen atoms kept at fixed distances were used as capping fragments. As an example, the electron density of the auxiliary molecular structures A, B, and C in Fig. S1 was employed to evaluate the EDS in TP using equation (1):

$$\mathrm{EDS(TP)} = \rho_{\mathrm{TP}} - \rho_{\mathrm{A}} - \rho_{\mathrm{B}} + \rho_{\mathrm{C}} \quad (1)$$

The EDS in intermolecular systems, such as the monohydrates of PBT and TP, was obtained as the difference of the electron density of the cluster minus the sum of that of the isolated monomers [48] as in equation (2).

$$\mathrm{EDS(Z{\cdots}H_2O)} = \rho_{\mathrm{Z{\cdots}H_2O}} - \rho_{\mathrm{Z}} - \rho_{\mathrm{H_2O}} \quad (2)$$

Finally, the Interactive Quantum Atom (IQA) methodology [49] was employed to compare the different components of the relative energies between the two isomers of TP and PBT. IQA provides both monoatomic and diatomic contributions to the electronic energy, and the sum of all these terms recovers the total electronic energy of the system. In total, 171 terms were evaluated for the TP molecules and 300 for the PBT ones. The program AIMAll [50] was used to evaluate the IQA partitioning and the quality of the numerical integration was verified by checking that the integrated Laplacian values remained small (<0.001 au) [51].

3. Results and discussion

3.1. Potential energy surface

The PES scans for TP and PBT are shown in Fig. 2 (B3LYP-D3(BJ)). Three stationary points were located on the profile, characterized by a vanishing gradient. To distinguish between minima and transition states, an analysis of the Hessian matrix was performed. For both molecules the two minima correspond to near-planar *zusammen* (*Z*) and *entgegen* (*E*) conformers, while the transition state occurs at the near-perpendicular dihedral. The separation between the two conformers is similar in both molecules and quite small (2.3-2.8 kJ mol^{-1} with B3LYP-D3(BJ) and B2PLYP-D3(BJ), but 1.3-1.6 kJ mol^{-1} using DLPNO-CCSD

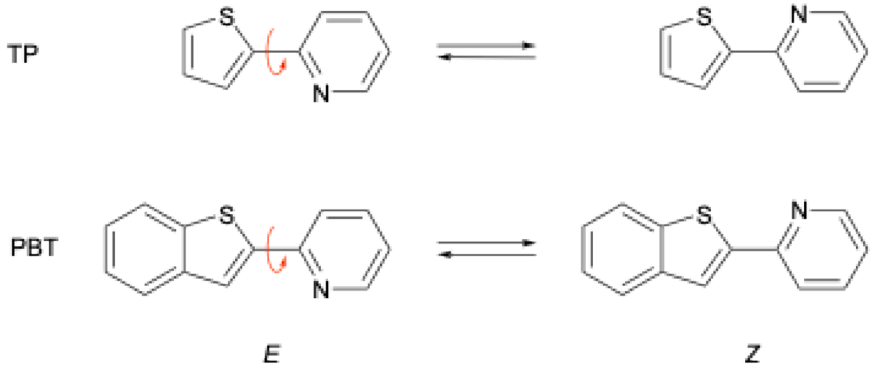

Fig. 1. The plausible *E* and *Z* conformations of 2-(2-thienyl)pyridine (TP) and 2-(2-pyridyl)benzothiophene (PBT).

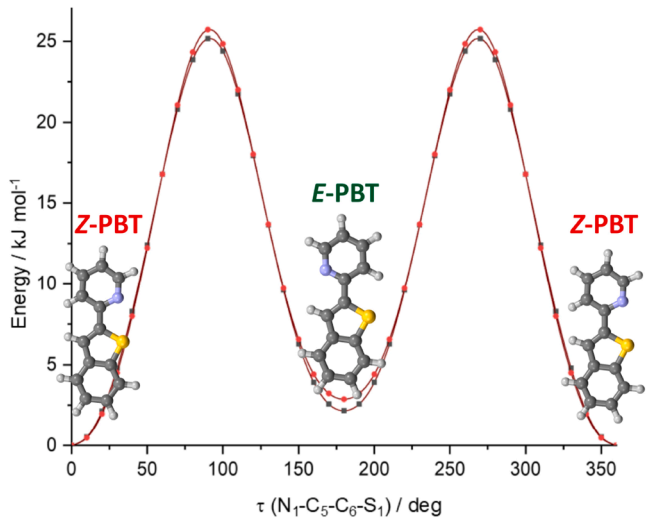

Fig. 2. The PES for 2-(2-thienyl)pyridine (TP, black trace) and 2-(2-pyridyl) benzothiophene (PBT, red trace) show their similarity for the interconversion between the *Z* and *E* conformers (B3LYP-D3(BJ)/def2-TZVP). The preferred conformations of PBT are shown for illustration.

(T), see Tables S1-S2 in Supporting information). In all cases the *Z* form is predicted as global minimum (unlike a previous B3LYP calculation [52]). The energy barrier for conformational interconversion (TP: 25.07 kJ mol^{-1}, PBT: 24.6 kJ mol^{-1} using B3LYP-D3(BJ)) is well above the empirical threshold (~4–5 kJ mol^{-1}) for efficient conformational relaxation under supersonic jet expansion [53,54]. This suggests that both conformers may be experimentally observable.

The PES of the monohydrates showed two preferred structures (*Z*-Wd and *E*-Wd) within a window of 3 kJ mol^{-1} (B3LYP-D3(BJ)), corresponding to microsolvation through the nitrogen group in the pyrimidinic moiety (Fig. 3 and Tables S3-S4). The water unit behaves as hydrogen bond donor (Wd), forming a conventional O-H···N hydrogen bond and secondary C-H···O interactions either with the pyridine ring or with the opposite ring for the *Z* and *E* isomers. The O-H···N interaction is

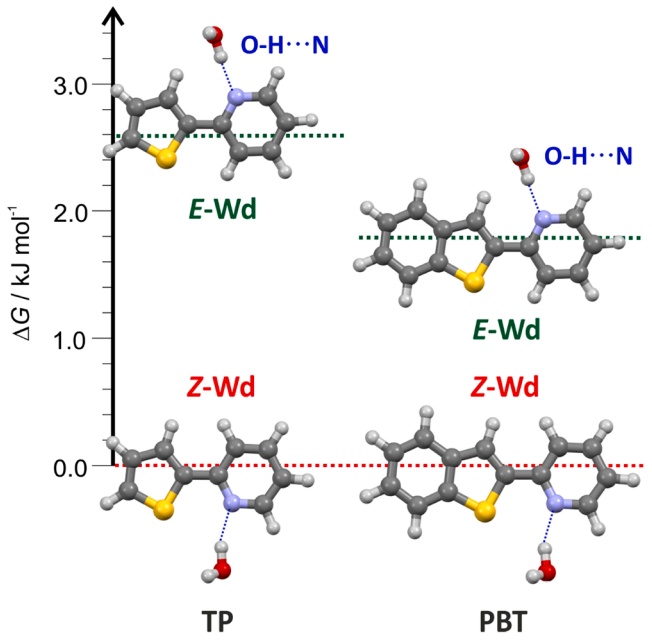

Fig. 3. The preferred monohydrates of 2-(2-thienyl)pyridine (TP···H_2O, left side) and 2-(2-pyridyl)benzothiophene (PBT···H_2O, right side) share the same O-H···N interaction (water proton donor or Wd) for both *Z* and *E* isomers.

similar to that observed in the pyridine monohydrate [55]. The third water monohydrate in PBT (PBT-Wπ) is higher in energy (6 kJ mol^{-1}) and corresponds to the interaction with the π-electron system of benzothiophene, forming O-H···π interaction. Similar interactions were observed in the monohydrates of benzofuran [56] and thiophene [57]. In the TP monohydrate the third isomer is much higher in energy (14 kJ mol^{-1}) and corresponds to a C-H···O interaction, with the water oxygen in the molecular plane. The calculated geometries are collected in Tables S5-S14. All these predictions require experimental validation, as factors such as carrier gas composition and the accuracy of theoretical models can influence the conformational equilibria.

3.2. Rotational spectra

The rotational spectra of the monomers and the monohydrates were recorded in successive experiments (Figs. 4 and S2). For both molecules two rotamers of the monomers and a single monohydrated species were assigned in the spectrum. In all cases the presence of a quadrupolar ^{14}N nucleus (I=1) introduces coupling effects associated to the molecular electric field gradient at the atom position, causing hyperfine splittings (Fig. 4). The rotational transitions were fitted to experimental accuracy using the Watson's semi-rigid rotor Hamiltonian (*S*-reduction and I^r representation) [58], comprising the rigid term ($\widehat{\boldsymbol{H}}_R$), the centrifugal distortion corrections ($\widehat{\boldsymbol{H}}_{CD}$), and the ^{14}N nuclear quadrupole coupling term ($\widehat{\boldsymbol{H}}_Q$) [59]. The calculations were implemented in Pickett's SPFIT program [60]. The monomers of TP and PBT turned out to be very rigid, and a satisfactory fit was obtained with only the rotational constants and the diagonal elements of the nuclear quadrupole coupling tensor, shown

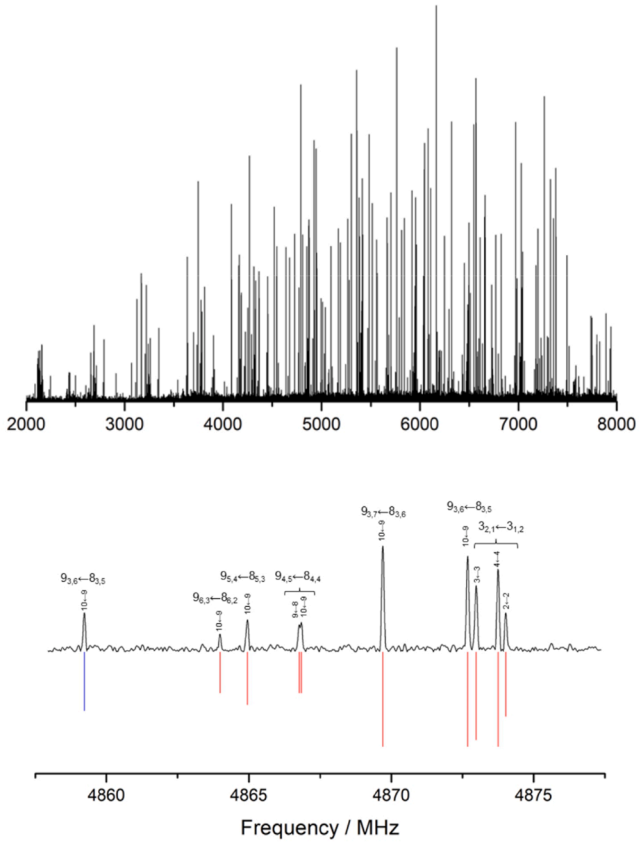

Fig. 4. The rotational spectrum of 2-(2-pyridyl)benzothiophene (PBT) and an enlarged frequency region illustrating typical rotational transitions of the *Z* (red) and *E* (blue) conformers and their hyperfine components (rotational quantum numbers and hyperfine components labeled as $J'_{K'_{-1},K'_{+1}} \leftarrow J_{K_{-1},K_{+1}}$ and $F' \leftarrow F$, respectively).

in Table 1. A comparison with the predicted parameters unequivocally assigned the carriers of the spectra to the *Z* and *E* species of TP and PBT. Assuming a linear dependence of the spectral intensities with the electric dipole moment a calculation of relative intensities for the *Z* and *E* species of PBT (52 transitions) and TP (38 transitions) yielded jet population ratios of $N_E/N_Z = 0.40$ and 0.27, respectively, for both monomers. This calculation is consistent with the relative energies predicted in Tables S1-S2, as it would result in Gibbs energies of 2.3 or 3.2 kJ mol^{-1}, respectively, at preexpansion temperatures (or smaller values for lower effective conformational temperatures).

$$\widehat{\boldsymbol{H}} = \widehat{\boldsymbol{H}}_R + \widehat{\boldsymbol{H}}_{CD} + \widehat{\boldsymbol{H}}_Q \quad (3)$$

The effective planarity of TP and PBT is confirmed by the values of the inertial defect $\Delta \left(= I_{cc} - I_{aa} - I_{bb} = -2P_c = -2\sum_{i=1}^{N} m_i c_i^2 \right)$ in Table 1, which, in the rigid rotor approximation, gives the mass extension out of the *ab* inertial plane. The small negative values (PBT: –1.01 to –1.08 uÅ^2; TP: –0.69 to –0.77 uÅ^2), larger than for the monomers (benzothiophene: -0.07 uÅ^2 [61]; pyridine: 0.04 uÅ^2 [62]; thiophene: 0.07 uÅ^2 [63]) are due to zero-point vibrational effects [64]. Harmonic vibrational frequency calculations confirm the existence of low-energy out-of-plane modes responsible for this behavior. In the case of PBT, the two lowest-frequency vibrations ($\nu_1 \approx 40$ cm^{-1} and $\nu_2 \approx 61$ cm^{-1}, see Fig. S3 and Tables S15-S16) involve torsional and bending motions between the two rigid moieties of pyridine and benzothiophene, displacing them out of the molecular plane in opposite directions. Similar modes are observed in TP. A comparison with the solid-state diffraction structures, slightly non-planar, is shown in Table S17.

The rotational spectra of the TP···H_2O and PBT···H_2O monohydrates were analyzed similarly. A single water dimer was detected for each molecule, which could be reproduced with the diagonal quadrupole coupling terms and one or two centrifugal distortion constants in Table 2. No tunelling effects were observed for the dimers, as expected from the assymetry of the cluster. A comparison with the computational predictions confirms that both monohydrates are built upon the *Z* conformer, with the water molecule acting as proton donor to the nitrogen atom through a O-H···N hydrogen bond. The inertial defects (PBT···H_2O: –2.56 uÅ^2; TP···H_2O: –1.80 uÅ^2) are larger than on other dimers with one water hydrogen atom out of the molecular plane (i.e., benzofuran···H_2O: -0.84 uÅ^2 [56]) or monohydrates assumed planar (i.e., pyrazine···H_2O: –0.51 uÅ^2 [65]), but probably compatible with geometries very close to planarity or very slightly tilted (<4° with B3LYP-D3(BJ)). By comparison, these values clearly differ from pyridine···H_2O (8.32 uÅ^2), which presents several coupled large amplitude motions [55]. All measured rotational transitions are available in Tables S18-S23. No additional species were assigned in this work.

3.3. Hyperconjugative and non-covalent interactions

We investigated the influence of hyperconjugative effects and non-covalent interactions in the stability of the monomers and monohydrates of TP and PBT using computational techniques. Initially, a Natural Bond Orbital (NBO) analysis was performed for both the *Z* and *E* conformers of the monomers (B3LYP-D3(BJ)/def2-TZVP). Despite the complexity of these heteroaromatic systems and the extensive electron delocalization inherent to their conjugated frameworks, specific donor–acceptor orbital effects emerged as particularly relevant. In both PBT and TP, a significant interaction exists between the nitrogen lone pair and the σ* antibonding orbital of the C–S bond or n(N)→ σ* (C-S), shown in Fig. S4 and Table S24. In the *Z* conformers, this effect is structurally favored due to the spatial proximity of the nitrogen and sulfur atoms (*Z*: 4.5 kJ mol^{-1} vs. *E*: 2.9 kJ mol^{-1}), promoting intramolecular electron donation and thus stabilizing this geometry over the *E* form. However, this effect is modest compared to other interactions from the lone pair-bearing nitrogen atom (i.e., lone pair donations to σ* (C6-C7) or σ*(C9-C10)), and their differential conformational contribution is small. Moreover, the sum of all stabilizing interactions (19.5 kJ mol^{-1}) is in any case larger than the conformational separation at the same calculation level (ca. 2.9 kJ mol^{-1}), suggesting compensating effects from other interactions.

Additional information was obtained from the predicted intramolecular EDS for the two conformers of TP and PBT, shown in Fig. 5. Two additional intermolecular systems with a prototypic chalcogen bond (pyridine···SF_2) and hydrogen bond (pyridine···HF) were included for comparison. The intramolecular EDS of the *Z* isomers clearly

Table 1
Experimental and theoretical spectroscopic parameters of the *Z* and *E* conformations of PBT and TP (B3LYP-D3(BJ)/def2-TZVP).

	Z-PBT		*E*-PBT		*Z*-TP		*E*-TP	
Parameter	Experiment[g]	B3LYP-D3(BJ)	Experiment	B3LYP-D3(BJ)	Experiment	B3LYP-D3(BJ)	Experiment	B3LYP-D3(BJ)
A / MHz [a]	1930.80601(24)	1938.8	1894.554(15)	1901.0	2836.93680(16)	2851.3	2824.89448(92)	2841.3
B / MHz	288.749090(38)	289.4	288.18105(19)	288.8	629.485482(40)	630.8	622.46918(34)	623.2
C / MHz	251.311710(36)	251.8	250.26778(17)	250.7	515.534582(44)	516.5	510.47225(28)	511.1
Δ / u Å^2	-1.0161(6)		-1.086(5)		-0.6862(1)		-0.773(1)	
D_J / kHz [b]	[0.0]	0.001	[0.0]	0.001	[0.0]	0.008	[0.0]	0.00674
D_{JK} / kHz	[0.0]	0.003	[0.0]	0.001	[0.0]	0.016	[0.0]	0.01600
D_K / kHz	[0.0]	0.111	[0.0]	0.118	[0.0]	0.160	[0.0]	0.15983
d_1 / kHz	[0.0]	-0.14	[0.0]	-0.15	[0.0]	-1.53	[0.0]	-1.37
d_2 / kHz	[0.0]	-0.01	[0.0]	-0.01	[0.0]	-0.17	[0.0]	-0.16
χ_{aa} / MHz [c]	-0.4280 (64)	-0.52	-0.6 (3)	-0.62	-0.8832(52)	-1.03	0.063(31)	0.06
χ_{bb} / MHz	-2.663(66)	-2.90	-2.56 (25)	-2.86	-2.1616(80)	-2.33	-3.142(39)	-3.50
χ_{cc} / MHz	3.091(66)	3.42	3.16 (25)	3.48	3.0448(80)	3.35	3.078(39)	3.43
$\lvert\mu_a\rvert$ / D [d]	Y	1.23	Y	0.96	Y	0.88	Y	0.48
$\lvert\mu_b\rvert$ / D	Y	2.06	Y	0.83	Y	1.85	Y	1.09
$\lvert\mu_c\rvert$ / D	N	0.00	N	0.00	N	0.00	N	0.00
ΔE_0 /kJ mol^{-1} [e]		0.00		2.27		0.00		2.87
ΔG / kJ mol^{-1}		0.00		2.03		0.00		2.55
σ / kHz [f]	8.7		8.9		14.4		13.3	
N	307		80		331		127	

[a] Rotational constants (*A, B, C*) and inertial defect ($\Delta = I_c - I_b - I_a$),
[b] Watson's *S*-reduction centrifugal distortion constants (D_J, D_{JK}, D_K, d_1, d_2),
[c] Nuclear quadrupole coupling tensor elements ($\chi_{\alpha,\beta}$, $\alpha,\beta = a, b, c$),
[d] Electric dipole moment components (μ_α, $\alpha = a, b, c$),
[e] Relative electronic energy including zero-point correction (ZPE) and Gibbs free energy (298 K, 1 atm).
[f] Number of transitions and root mean square deviation of the fit.
[g] Standard errors in parentheses in units of the last digit.

Table 2
Spectroscopic parameters of the monohydrates PBT···H_2O and TP···H_2O (B3LYP-D3(BJ)/def2-TZVP calculation level).

	PBT···H2O				TP···H2O			
	Experiment	*Z*-Wd	*E*-Wd	*E*-Wπ	Experiment	*Z*-Wd	*E*-Wd	*E*-Ws
A / MHz [a]	1003.41133(48)	1016.6	980.7	1192.1	1188.9321(17)	1213.4	1180.8	1083.89
B / MHz	272.34958(18)	274.8	280.5	248.3	616.05040(60)	620.6	609.1	618.79
C / MHz	214.44097(17)	216.6	219.1	235.3	406.37682(34)	411.1	404.0	394.69
Δ / u Å^2	-2.599(3)				-1.801(2)			
D_J / kHz	0.00216(61)	0.001	0.001	0.014	[0.0]	0.183	0.140	0.22886
D_{JK} / kHz	0.0543(56)	0.081	0.042	0.377	0.396(54)	-0.277	-0.209	-0.32259
D_K / kHz	[0.0]	0.035	0.050	-0.064	[0.0]	0.101	0.076	0.10204
d_1 / Hz	[0.0]	-0.34	-0.11	-0.63	[0.0]	-55.61	-43.71	-101.73
d_2 / Hz	[0.0]	-0.40	-0.31	1.67	[0.0]	27.56	18.92	6.68
χ_{aa} / MHz	0.26(2)	0.21	0.07	-0.66	0.24(6)	-0.29	0.80	0.36
χ_{bb} / MHz	-3.09(2)	-3.25	-3.06	-2.69	-2.77(7)	-2.67	-3.76	-3.78
χ_{cc} / MHz	2.83(2)	3.03	3.00	3.35	2.53(7)	2.95	2.96	3.44
$\lvert\mu_a\rvert$ / D	Y	0.58	0.94	1.98	N	0.34	0.13	1.12
$\lvert\mu_b\rvert$ / D	Y	4.18	2.93	1.02	Y	4.07	3.27	0.34
$\lvert\mu_c\rvert$ / D	N	0.97	1.10	2.09	N	1.12	1.22	0.00
ΔE_0 / kJ mol^{-1}		1.19	0.00	12.32		0.34	0.00	18.21
ΔG / kJ mol^{-1}		0.00	1.77	5.77		0.00	2.55	14.05
ΔE_B / kJ mol^{-1} [b]		-29.8	-35.8	-16.9		-30.1	-35.7	-12.2
σ / kHz	11.7				16.3			
N	196				70			

[a] Parameter definition as in Table 1.
[b] Complexation energy including the basis set superposition error (BSSE) correction.

resemble that of the intermolecular chalcogen bond in pyridine···SF_2. However, the effect of the interaction in the electron density is clearly smaller in the intramolecular case than in the intermolecular one as indicated by the different isosurfaces (intramolecular: ± 0.001 au; intermolecular: ±0.002 au). Similar results are obtained for the *E* isomers in comparison with the intermolecular hydrogen bonded system of pyridine···HF.

The relative contributions of the different IQA energy terms for the *E* and *Z* conformers were also compared, yielding very similar trends for both TP and PBT. The main factors stabilizing the *Z* conformers are the N···S interaction (+92 and +93 kJ mol^{-1} for TP and PBT, respectively) and the S–C(5) bond (+30 and +26 kJ mol^{-1}, respectively). The former corresponds to the chalcogen bond interaction, whereas the latter reflects the increased S–C(5) bond charge arising from donation of the nitrogen lone pair into the σ* S–C(5) antibonding orbital, in agreement with the NBO analysis. Conversely, the intraatomic energy of the sulfur atom favors the *E* conformer by 59 and 58 kJ mol^{-1} for TP and PBT, respectively. This stabilization arises from the less positive atomic charge on sulfur in the *E* conformer compared to the *Z* form. In addition, the N–H interatomic interaction contributes a further 42 and 43 kJ mol^{-1} in favor of the *E* conformer, consistent with an incipient hydrogen-bond-like contact. The dispersion contribution is essentially the same for both conformers, differing by less than 0.2 kJ mol^{-1} (B3LYP-D3(BJ)/def2-TZVP). As a result, the larger stability of the *Z* form should be attributed to a combination of electronic delocalization and non-covalent attractive interactions, including the contributions of the N···S chalcogen bond.

The presence of intra- and intermolecular non-covalent interactions (NCI) in the monohydrates was mapped using an analysis of the reduced gradient (s) of the electronic density (ρ), introduced by Johnson and Contreras [46]:

$$s = \frac{1}{2(3\pi^2)^{1/3}} \frac{|\nabla\rho|}{\rho^{4/3}} \quad (4)$$

Abrupt variations in the reduced gradient between interacting atoms reveal critical points that signal the presence of intra- or intermolecular interactions. The NCI plot in Figs. 6 and S6 highlight the regions of low electron density and small gradient magnitudes, which correspond to weak interactions. To distinguish between attractive and repulsive interactions, the reduced gradient is plotted against the electron density multiplied by the sign of the second eigenvalue of the electron density Hessian matrix (λ_2).

For both the *Z* and *E* isomers of monohydrated PBT and TP, the NCI and EDS plots (Figs. 6 and S7) clearly reveals the presence of the moderate O-H···N hydrogen bond between water and the nitrogen atom of the heterocycle. In contrast, the higher energy complex of PBT-*E*-Wπ), in which water interacts with the π-system, shows only diffuse, long-range electrostatic interactions and lacks a defined attractive region on the isosurface maps. This observation is qualitatively consistent with the higher relative energies obtained from quantum chemical calculations. Additionally, the NCI analysis confirms secondary interactions such as C-H···O hydrogen bonds involving hydrogen atoms from the TP or PBT backbone and other weak interactions, which might influence the stabilization and conformational preferences of the complexes. Weak interactions are also noticed in the region between the nitrogen and sulfur atoms for the *Z* form, suggesting a possible contribution to molecular stability.

4. Conclusions

We analyzed the potential energy surface, stereochemistry and non-covalent interactions in 2-(2-thienyl)pyridine, 2-(2-pyridyl)benzothiophene and their monohydrates, using a combination of rotational data and first principles calculations. Two planar isomers were detected in the gas phase for both monomers, corresponding to the *Z* and *E* conformations. The monohydrated species maintain the preferred *Z* structure of the monomer with slight torsional distortions and confirm that solvation is primary directed to the nitrogen atom in the pyrimidine unit through a O-H···N hydrogen bond. As observed in other gas-phase water clusters, these experiments highlight the dominant role of the directional hydrogen bond in stabilizing the hydrated adducts, simultaneously emphasizing the interplay between various weak interactions in dictating their geometry and relative energies.

Accurate rotational parameters were derived for all the observed species, including the nuclear quadrupole coupling constants caused by the ^{14}N nuclei, which are highly sensitive to the electronic environment around the quadrupolar nucleus. The (D3) dispersion-corrected hybrid (B3LYP) and double-hybrid (B2PLYP) satisfactorily agree with the experiment. Additional energy calculations were extended to the RI-MP2 and the DLPNO-CCSD(T) level. Initial hypotheses on the relevance of donor–acceptor electronic effects between the nitrogen and sulfur atom in the *Z* global minimum are not confirmed by the NBO

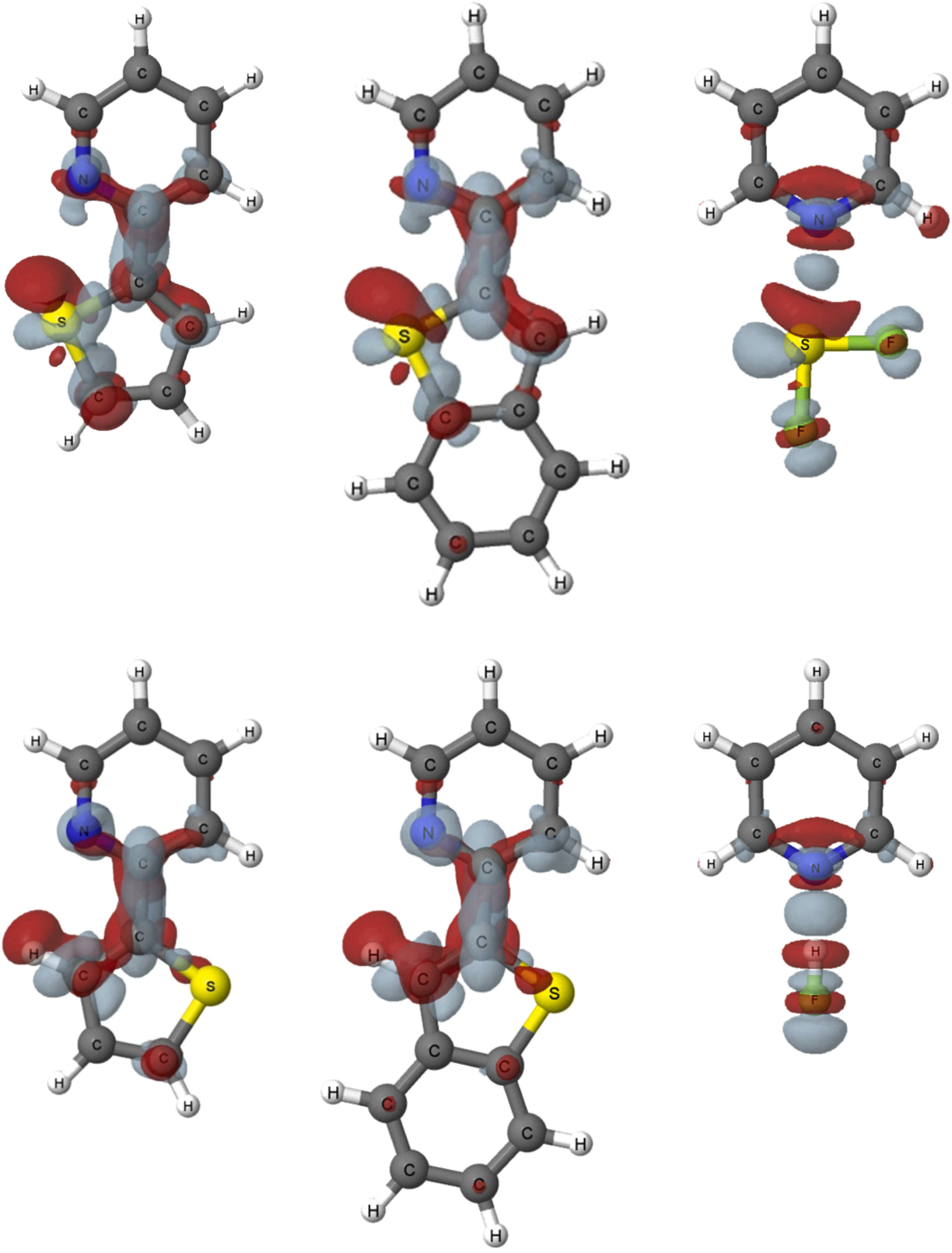

Fig. 5. Electronic density shift representations for TP, PBT, pyridine···SF_2 and pyridine···HF. Green and red surfaces indicate regions of gain and loss of electron density due to the interaction of the two rings. The isosurfaces have values of ±0.001 au for the monomers and ±0.002 au for the dimers.

calculations, which suggest that other electron delocalizations and a N···S chalcogen non-covalent interactions additionally contribute to the conformational equilibrium. The observed stereochemistry of TP and PBT is consistent with previously reported behavior in related systems, including 2-(2-pyridyl)indole and its pharmacologically relevant analogues. In those cases, classical N-H···N or N-H···π hydrogen bonds dominate the conformational preferences of the monomers. In the title compounds the absence of polar protons reveals how electron

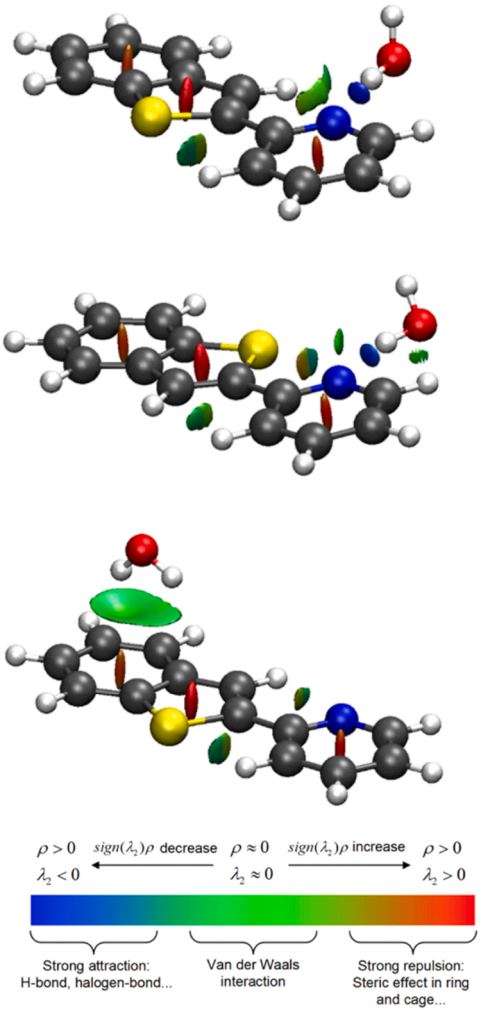

Fig. 6. Non-covalent interaction plots [46] for the most stable monohydrates of 2-(2-thienyl)pyridine (PBT). The regions associated to stronger attractive interactions, specifically the O-H···N hydrogen bond, are colored in blue.

delocalization may fulfill a similar geometric role without introducing additional hydrogen bonding. The presence of intramolecular interactions between heteroatoms may be advantageous in medicinal chemistry contexts and a relevant molecular factor for the design new drugs. In particular, the suppression of hydrogen bonding can be beneficial for blood–brain barrier permeability, making these scaffolds interesting isosteric replacements for classical hydrogen-bond-rich pharmacophores. Finally, the present work highlights the important role of gas phase studies to discern the molecular role and intra and intermolecular interactions on biologically and pharmacollogically relevant molecules.

CRediT authorship contribution statement

Domingo Heras: Writing – review & editing, Visualization, Validation, Software, Investigation, Formal analysis. **Wenqin Li:** Writing – review & editing, Investigation. **Ibon Alkorta:** Investigation, Software, Writing – review & editing. **Ruth Pinacho:** Writing – review & editing, Software, Investigation. **Lourdes Enríquez:** Writing – review & editing, Software, Investigation. **J. Emiliano Rubio:** Writing – review & editing, Software, Investigation. **Cristóbal Pérez:** Writing – review & editing, Validation, Supervision, Methodology, Investigation, Funding acquisition, Formal analysis, Conceptualization. **Alberto Lesarri:** Writing – review & editing, Writing – original draft, Validation, Supervision, Methodology, Investigation, Funding acquisition, Formal analysis, Conceptualization.

Declaration of competing interest

The authors declare that they have no known competing financial interests or personal relationships that could have appeared to influence the work reported in this paper.

Acknowledgments

We thank Prof. Dr. Martín Jaraíz for critically reading the manuscript and discussions. W.L. thanks the Chinese Scholarship Council for a research grant. Funding from the Spanish *Ministerio de Ciencia, Innovación y Universidades* (MICIU) and the European Regional Development Fund (ERDF) under grants PID2021-125015NB-I00 and PID2024-158277NB-I00 is gratefully acknowledged. C.P. thanks the ERC for the CoG HydroChiral (Grant Agreement No 101124939).

Supplementary materials

Supplementary material associated with this article can be found, in the online version, at doi:10.1016/j.jqsrt.2026.109857.

Data availability

The data that support the findings of this study are available within the article and its supplementarymaterial or on request from the corresponding author.

References

[1] Shipman ST, Pate BH. New Techniques in Microwave Spectroscopy. In: Merkt F, Quack M, editors. Handbook of High-resolution Spectroscopy. New York: John Wiley & Sons, Ltd; 2011. p. 801–28. https://doi.org/10.1002/9780470749593.hrs036.
[2] Grabow J-U. Fourier Transform Microwave Spectroscopy Measurement and Instrumentation. In: Merkt F, Quack M, editors. Handbook of High-resolution Spectroscopy. New York: John Wiley & Sons, Ltd; 2011. p. 723–99. https://doi.org/10.1002/9780470749593.hrs037.
[3] Shubert VA, Schmitz D, Patterson D, Doyle JM, Schnell M. Identifying Enantiomers in Mixtures of Chiral Molecules with Broadband Microwave Spectroscopy. Angew Chem Int Ed 2014;53:1152–5. https://doi.org/10.1002/anie.201306271.
[4] Domingos SR, Pérez C, Schnell M. Sensing Chirality with Rotational Spectroscopy. Annu Rev Phys Chem 2018;69:499–519. https://doi.org/10.1146/annurev-physchem-052516-050629.
[5] Pate BH, Evangelisti L, Caminati W, Xu Y, Thomas J, Patterson D, et al. Quantitative chiral analysis by molecular rotational spectroscopy. Chiral Analysis: Advances in Spectroscopy, Chromatography and Emerging Methods: Second Edition. Second Edi. Elsevier B.V.; 2018. p. 679–729. https://doi.org/10.1016/B978-0-444-64027-7.00019-7.
[6] Neill JL, Evangelisti L, Pate BH. Analysis of isomeric mixtures by molecular rotational resonance spectroscopy. Anal Sci Adv 2023;4:204–19. https://doi.org/10.1002/ansa.202300021.
[7] Wahab MF, Aslani S, Mikhonin AV, Neill JL, Armstrong DW. Enhancing Sensitivity for High-Selectivity Gas Chromatography-Molecular Rotational Resonance Spectroscopy. Anal Chem 2021;93:15525–33. https://doi.org/10.1021/acs.analchem.1c03710.
[8] Dabbs JD, Taylor CC, Holdren MS, Brewster SE, Quillin BT, Meng AQ, et al. Designing chemical systems for precision deuteration of medicinal building blocks. Nat Commun 2024;15:8473. https://doi.org/10.1038/s41467-024-52127-6.
[9] Pérez C, Zaleski DP, Seifert NA, Temelso B, Shields GC, Kisiel Z, et al. Hydrogen Bond Cooperativity and the Three-Dimensional Structures of Water Nonamers and Decamers. Angew Chem Int Ed 2014;53:14368–72. https://doi.org/10.1002/anie.201407447.
[10] Steber AL, Hussain FS, Lesarri A, Zwier TS, Pate BH, Evangelisti L, et al. Water Cooperativity Impacts Aromatic Interactions in the Aggregation of Benzene with Water. J Am Chem Soc 2025;147:19568–74. https://doi.org/10.1021/jacs.4c17315.
[11] Pinacho P, Pérez C, Stahn M, Saragi RT, Hansen A, Grimme S, et al. Hydrogen Bond Interaction Networks in the Mixed Pentamers of Hydrogen Sulfide and Water. J Am Chem Soc 2025;147:18576–82. https://doi.org/10.1021/jacs.4c18276.
[12] Keri RS, Chand K, Budagumpi S, Balappa Somappa S, Patil SA, Nagaraja BM. An overview of benzo [b] thiophene-based medicinal chemistry. Eur J Med Chem 2017;138:1002–33. https://doi.org/10.1016/j.ejmech.2017.07.038.

[13] Thakur S, Kumar D, Jaiswal S, Goel KK, Rawat P, Srivastava V, et al. Medicinal chemistry-based perspectives on thiophene and its derivatives: exploring structural insights to discover plausible druggable leads. RSC Med Chem 2025;16:481–510. https://doi.org/10.1039/D4MD00450G.

[14] Dömötör O, Teixeira RG, Spengler G, Avecilla F, Marques F, Lenis-Rojas OA, et al. Ruthenium(II) polypyridyl complexes with benzothiophene and benzimidazole derivatives: Synthesis, antitumor activity, solution studies and biospeciation. J Inorg Biochem 2023;238:112058. https://doi.org/10.1016/j.jinorgbio.2022.112058.

[15] Cano C, Saravanan K, Bailey C, Bardos J, Curtin NJ, Frigerio M, et al. 1-Substituted (Dibenzo[b,d]thiophen-4-yl)-2-morpholino-4H-chromen-4-ones Endowed with Dual DNA-PK/PI3-K Inhibitory Activity. J Med Chem 2013;56:6386–401. https://doi.org/10.1021/jm400915j.

[16] Morales-Tenorio M, Lasala F, Garcia-Rubia A, Aledavood E, Heung M, Olal C, et al. Discovery of Thiophene Derivatives as Potent, Orally Bioavailable, and Blood–Brain Barrier-Permeable Ebola Virus Entry Inhibitors. J Med Chem 2024;67:16381–402. https://doi.org/10.1021/acs.jmedchem.4c01267.

[17] Lalevée J, Mokbel H, Fouassier J-P. Recent Developments of Versatile Photoinitiating Systems for Cationic Ring Opening Polymerization Operating at Any Wavelengths and under Low Light Intensity Sources. Molecules 2015;20:7201–21. https://doi.org/10.3390/molecules20047201.

[18] Delogu G, Begala M, Matos M, Cruciti D, Sogos V, Era B, et al. A New Class of Benzo[b]thiophene-chalcones as Cholinesterase Inhibitors: Synthesis, Biological Evaluation, Molecular Docking and ADME Studies. Molecules 2024;29:3748. https://doi.org/10.3390/molecules29163748.

[19] Zhang P, Jacques P-A, Chavarot-Kerlidou M, Wang M, Sun L, Fontecave M, et al. Phosphine Coordination to a Cobalt Diimine–Dioxime Catalyst Increases Stability during Light-Driven H $_2$ Production. Inorg Chem 2012;51:2115–20. https://doi.org/10.1021/ic2019132.

[20] Capodilupo AL, Fabiano E, De Marco L, Ciccarella G, Gigli G, Martinelli C, et al. [1]Benzothieno[3,2-b]benzothiophene-Based Organic Dyes for Dye-Sensitized Solar Cells. J Org Chem 2016;81:3235–45. https://doi.org/10.1021/acs.joc.6b00192.

[21] Zhao Q, Huang C, Li F. Phosphorescent heavy-metal complexes for bioimaging. Chem Soc Rev 2011;40:2508. https://doi.org/10.1039/c0cs00114g.

[22] Prier CK, Rankic DA, MacMillan DWC. Visible Light Photoredox Catalysis with Transition Metal Complexes: Applications in Organic Synthesis. Chem Rev 2013;113:5322–63. https://doi.org/10.1021/cr300503r.

[23] Bringmann G, Günther C, Ochse M, Schupp O, Tasler S. Biaryls in Nature: A Multi-Facetted Class of Stereochemically, Biosynthetically, and Pharmacologically Intriguing Secondary Metabolites. Fortschritte der Chemie organischer Naturstoffe. Wien: Springer-Verlag; 2001. p. 1–249. https://doi.org/10.1007/978-3-7091-6227-9_1.

[24] Eliel EL, Wilen SH. Stereochemistry of Organic Compounds. New York, NY: John Wiley & Sons, Inc; 1994.

[25] Kottas GS, Clarke LI, Horinek D, Michl J. Artificial Molecular Rotors. Chem Rev 2005;105:1281–376. https://doi.org/10.1021/cr0300993.

[26] Ottaviani P, Maris A, Caminati W. Atropisomerism in bisphenols: Free jet absorption millimeter wave study of 2,2′-biphenol. J Mol Struct 2004;695–696:353–6. https://doi.org/10.1016/j.molstruc.2003.12.048.

[27] Uriarte I, Pérez C, Caballero-Mancebo E, Basterretxea FJ, Lesarri A, Fernández JA, et al. Structural Studies of Nicotinoids: Cotinine versus Nicotine. Chem - Eur J 2017;23:7238–44. https://doi.org/10.1002/chem.201700023.

[28] Lesarri A, Cocinero EJ, Evangelisti L, Suenram RD, Caminati W, Grabow J-U. The conformational landscape of nicotinoids: Solving the conformational disparity of anabasine. Chem - Eur J 2010;16:10214–9. https://doi.org/10.1002/chem.201000849.

[29] Écija P, Cocinero EJ, Lesarri A, Fernández JA, Caminati W, Castaño F. Rotational spectroscopy of antipyretics: Conformation, structure, and internal dynamics of phenazone. J Chem Phys 2013;138. https://doi.org/10.1063/1.4794693.

[30] Desyatnyk O, Pszczółkowski L, Thorwirth S, Krygowski TM, Kisiel Z. The rotational spectra, electric dipole moments and molecular structures of anisole and benzaldehyde. Phys Chem Chem Phys 2005;7:1708–15. https://doi.org/10.1039/B501041A.

[31] Neill JL, Shipman ST, Alvarez-Valtierra L, Lesarri A, Kisiel Z, Pate BH. Rotational spectroscopy of iodobenzene and iodobenzene–neon with a direct digital 2–8GHz chirped-pulse Fourier transform microwave spectrometer. J Mol Spectrosc 2011;269:21–9. https://doi.org/10.1016/j.jms.2011.04.016.

[32] Park GB, Field RW. Perspective: The first ten years of broadband chirped pulse Fourier transform microwave spectroscopy. J. Chem. Phys. 2016;144:200901. https://doi.org/10.1063/1.4952762.

[33] Bannwarth C, Ehlert S, Grimme S. GFN2-xTB—An Accurate and Broadly Parametrized Self-Consistent Tight-Binding Quantum Chemical Method with Multipole Electrostatics and Density-Dependent Dispersion Contributions. J Chem Theory Comput 2019;15:1652–71. https://doi.org/10.1021/acs.jctc.8b01176.

[34] Pracht P, Grimme S, Bannwarth C, Bohle F, Ehlert S, Feldmann G, et al. CREST—A program for the exploration of low-energy molecular chemical space. J Chem Phys 2024;160. https://doi.org/10.1063/5.0197592.

[35] Becke AD. Density-functional thermochemistry. III. The role of exact exchange. J Chem Phys 1993;98:5648–52. https://doi.org/10.1063/1.464913.

[36] Weigend F, Ahlrichs R. Balanced basis sets of split valence, triple zeta valence and quadruple zeta valence quality for H to Rn: Design and assessment of accuracy. Phys Chem Chem Phys 2005:3297–305. https://doi.org/10.1039/b508541a.

[37] Grimme S, Ehrlich S, Goerigk L. Effect of the damping function in dispersion corrected density functional theory. J Comput Chem 2011;32:1456–65. https://doi.org/10.1002/jcc.21759.

[38] Johnson ER, Becke AD. A post-Hartree-Fock model of intermolecular interactions: Inclusion of higher-order corrections. J Chem Phys 2006;124. https://doi.org/10.1063/1.2190220.

[39] Grimme S. Semiempirical hybrid density functional with perturbative second-order correlation. J Chem Phys 2006;124. https://doi.org/10.1063/1.2148954.

[40] Frisch MJ, Trucks GW, Schlegel HB, Scuseria GE, Robb MA, Cheeseman JR, et al. Gaussian 16, rev. C.01 2016.

[41] Riley KE, Platts JA, Řezáč J, Hobza P, Hill JG. Assessment of the performance of MP2 and MP2 variants for the treatment of noncovalent interactions. J Phys Chem A 2012;116:4159–69. https://doi.org/10.1021/jp211997b.

[42] Liakos DG, Guo Y, Neese F. Comprehensive benchmark results for the domain based local pair natural orbital coupled cluster method (DLPNO-CCSD(T)) for closed- and open-shell systems. J Phys Chem A 2020;124:90–100. https://doi.org/10.1021/acs.jpca.9b05734.

[43] Boys SF, Bernardi F. The calculation of small molecular interactions by the differences of separate total energies. Some procedures with reduced errors. Mol Phys 1970;19:553–66. https://doi.org/10.1080/00268977000101561.

[44] Neese F. Software update: The ORCA program system—Version 5.0. WIREs Comput Mol Sci 2022;12. https://doi.org/10.1002/wcms.1606.

[45] Glendening ED, Landis CR, Weinhold F. NBO 7.0 : New vistas in localized and delocalized chemical bonding theory. J Comput Chem 2019;40:2234–41. https://doi.org/10.1002/jcc.25873.

[46] Contreras-García J, Johnson ER, Keinan S, Chaudret R, Piquemal J-P, Beratan DN, et al. NCIPLOT: A Program for Plotting Noncovalent Interaction Regions. J Chem Theory Comput 2011;7:625–32. https://doi.org/10.1021/ct100641a.

[47] Sánchez-Sanz G, Trujillo C, Alkorta I, Elguero J. Electron density shift description of non-bonding intramolecular interactions. Comput Theor Chem 2012;991:124–33. https://doi.org/10.1016/j.comptc.2012.04.007.

[48] Iribarren I, Sánchez-Sanz G, Alkorta I, Elguero J, Trujillo C. Evaluation of Electron Density Shifts in Noncovalent Interactions. J Phys Chem A 2021;125:4741–9. https://doi.org/10.1021/acs.jpca.1c00830.

[49] Blanco MA, Martín Pendás A, Francisco E. Interacting quantum atoms: a correlated energy decomposition scheme based on the quantum theory of atoms in molecules. J Chem Theory Comput 2005;1:1096–109. https://doi.org/10.1021/ct0501093.

[50] Keith TA. AIMAll (Version 19.10.12), 2019 (aim.tkgristmill.com) 2019.

[51] Alkorta I, Picazo Ó. Influence of protonation on the properties derived from electron density. ARKIVOC 2005;ix:305–20. https://doi.org/10.3998/ark.5550190.0006.926.

[52] Lu Y-P, Ehara M. Electronic structure and optical properties of chelating heteroatomic conjugated molecules: a SAC-CI study. Theor Chem Acc 2009;124:395–408. https://doi.org/10.1007/s00214-009-0629-6.

[53] Felder P, Günthard HsH. Conformational interconversions in supersonic jets: Matrix IR spectroscopy and model calculations. Chem Phys 1982;71:9–25. https://doi.org/10.1016/0301-0104(82)87002-X.

[54] Ruoff RS, Klots TD, Emilsson T, Gutowsky HS. Relaxation of conformers and isomers in seeded supersonic jets of inert gases. J Chem Phys 1990;93:3142–50. https://doi.org/10.1063/1.458848.

[55] Mackenzie RB, Dewberry CT, Cornelius RD, Smith CJ, Leopold KR. Multidimensional Large Amplitude Dynamics in the Pyridine–Water Complex. J Phys Chem A 2017;121:855–60. https://doi.org/10.1021/acs.jpca.6b11255.

[56] Huang H, Li X, Feng G. Rotational spectroscopy of the benzofuran–water complex: Conformations and preferred noncovalent interactions. J Mol Spectrosc 2025;407:111979. https://doi.org/10.1016/j.jms.2024.111979.

[57] Silva WGDP, van Wijngaarden J. Characterization of Large-Amplitude Motions and Hydrogen Bonding Interactions in the Thiophene–Water Complex by Rotational Spectroscopy. J Phys Chem A 2021;125:3425–31. https://doi.org/10.1021/acs.jpca.1c02086.

[58] Watson J. Vibrational spectra and structure, 6. Amsterdam: Elsevier; 1977. p. 1–89.

[59] Gordy W, Cook R. Microwave Molecular Spectra. John Wiley & Sons; 1984.

[60] Pickett HM. The fitting and prediction of vibration-rotation spectra with spin interactions. J Mol Spectrosc 1991;148:371–7. https://doi.org/10.1016/0022-2852(91)90393-O.

[61] Welzel A, Stahl W. The FT microwave spectrum of benzo[b]thiophene: first application of a new heatable beam nozzle. Phys Chem Chem Phys 1999;1:5109–12. https://doi.org/10.1039/a906591a.

[62] Zdanovskaia MA, Esselman BJ, Kougias SM, Atwood MG, Jones GH, Stanton JF, et al. Precise Semi-Experimental Equilibrium (re SE) Structure of Pyridine from 32 Isotopologues: Accurate Assessment of the Effect of Nitrogen-Atom Substitution in Aromatic Rings. J Phys Chem A 2025;129:10737–50. https://doi.org/10.1021/acs.jpca.5c07184.

[63] Esselman BJ, Atwood MG, Nguyen HVL, Stanton JF, Woods RC, McMahon RJ. Semi-experimental equilibrium structure (re SE) of thiophene: Attempting to resolve the heavy-atom problem with 46 isotopologues. J Chem Phys 2025;163. https://doi.org/10.1063/5.0292964.

[64] Oka T. On negative inertial defect. J Mol Struct 1995;352–353:225–33. https://doi.org/10.1016/0022-2860(95)08844-L.

[65] Caminati W, Favero LB, Favero PG, Maris A, Melandri S. Intermolecular Hydrogen Bonding between Water and Pyrazine. Angew Chem Int Ed 1998;37:792–5. https://doi.org/10.1002/(SICI)1521-3773(19980403)37:6<792::AID-ANIE792>3.0.CO;2-R.